

Contact-Aware Non-prehensile Robotic Manipulation for Object Retrieval in Cluttered Environments

Yongpeng Jiang*, Yongyi Jia*, and Xiang Li

Abstract—Non-prehensile manipulation methods usually use a simple end effector, e.g., a single rod, to manipulate the object. Compared to the grasping method, such an end effector is compact and flexible, and hence it can perform tasks in a constrained workspace; As a trade-off, it has relatively few degrees of freedom (DoFs), resulting in an under-actuation problem with complex constraints for planning and control. This paper proposes a new non-prehensile manipulation method for the task of object retrieval in cluttered environments, using a rod-like pusher. Specifically, a candidate trajectory in a cluttered environment is first generated with an improved Rapidly-Exploring Random Tree (RRT) planner; Then, a Model Predictive Control (MPC) scheme is applied to stabilize the slider’s poses through necessary contact with obstacles. Different from existing methods, the proposed approach is with the contact-aware feature, which enables the synthesized effect of active removal of obstacles, avoidance behavior, and switching contact face for improved dexterity. Hence both the feasibility and efficiency of the task are greatly promoted. The performance of the proposed method is validated in a planar object retrieval task, where the target object, surrounded by many fixed or movable obstacles, is manipulated and isolated. Both simulation and experimental results are presented.

I. INTRODUCTION

Manipulation in clutter is a skill commonly demanded in daily life and production, such as desktop arrangement and tidying up open shelves. Such a task is challenging for a robot manipulator because the dexterity of the robot end effector is often restricted by the cluttered environment and unknown object properties. For example, the stable grasp pose might be occluded by surrounding obstacles; Another example is that fragile or heavy objects are generally dangerous to lift up. Non-prehensile manipulation proposed by Mason [1] only requires no penetration constraints and does not rely on stable grasping [2], which is suitable for performing tasks in cluttered environments.

This paper considers a representative and illustrative scenario in the problem of non-prehensile manipulation, that is, retrieving a target object from clutter with a single rod-like pusher overhead, as seen in Fig. 1. To achieve it, the pusher should contact and move the object (i.e., the planar slider) to the goal location in the presence of multiple obstacles. Such a task is not trivial, and the challenges can be summarized from the following aspects.

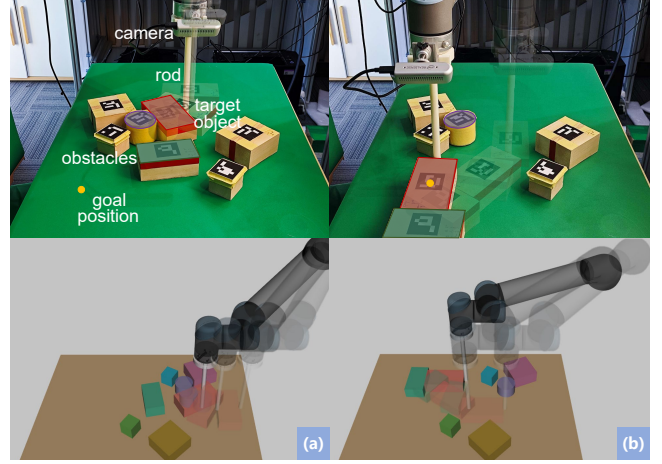


Fig. 1. **Object retrieval task through planar pushing.** The target object in red is separated from the clutter with a rod-like pusher through pushing manipulation. **Top:** camera view. **Bottom:** 3D visualization. **Left:** The purple cylinder is pushed aside and thus the target object quickly navigates through fixed obstacles on both sides. **Right:** the cyan cube is pushed away and thus the target object bursts through the clutter.

- The pusher and slider correlated by frictional contacts form an underactuated system with hybrid dynamics (i.e., alterable contact faces and modes), thus imposing complex kinodynamic constraints on planning and control.
- Push planning in cluttered environments is limited by the widely known narrow corridor problem, which seriously restricts solving efficiency.

To address the problems above, existing methods add extra constraints to reduce the search space, such as demanding the contact mode to be consistent [3] or limiting the slider’s movement to a particular pattern (i.e., Dubins path) [4]. However, such methods fail to sufficiently explore the state space, which might affect the solution quality. Besides, most existing works consider avoidance of simple obstacles [5] or implicitly assume an open space is required [3], [6]. However, in cluttered environments, there might be no feasible path to the goal position if the manipulated object merely avoids obstacles, or the total efficiency is unacceptable as it might take a long time to complete all the avoidance.

To improve the feasibility and efficiency of object retrieval in cluttered environments, this paper proposes a contact-aware non-prehensile manipulation method using the rod-like pusher, which integrates multiple actions of active removal of obstacles, avoidance behavior, and switching contact face to create a feasible path to the goal position if it is not

* Equal contribution

Y. Jiang, Y. Jia, and X. Li are with the Department of Automation, Tsinghua University, China. This work was supported in part by the National Natural Science Foundation of China under Grant U21A20517 and 52075290, and in part by the Science and Technology Innovation 2030-Key Project under Grant 2021ZD0201404. Corresponding author: Xiang Li (xiangli@tsinghua.edu.cn)

available at the beginning. The proposed method is organized as follows.

- For global motion planning, an RRT planner guided by reachable sets is proposed to generate candidate trajectories for the target object and enables flexible choice of contact faces and modes for improved dexterity.
- For local motion planning, an interaction model with necessary simplifications is applied to predict the outcome of the contacts between objects and then generate the safe and reliable active pushing action.
- For motion and interaction control, an MPC scheme stabilizes the object's pose around the candidate trajectory while navigating towards the goal, even during contact with obstacles.

Such a contact-aware feature allows the robot to explore different actions to generate more opportunities in cluttered environments. Moreover, the simplification of pushing dynamics yields reachable sets and object interaction model, which efficiently guide motion planning. Simulation results and further robot experiments are presented to verify the effectiveness of the proposed method.

II. RELATED WORKS

A. Non-prehensile Pushing Manipulation

Planar pushing [7] has recently become a representative task for developing non-prehensile manipulation algorithms. Modeling the pushing task needs to deal with the full relation between slide motion and frictional load. Several contributions in this field are summarized below, which have made the task increasingly tractable. Mason made the widely used quasi-static assumption [7]; Goyal *et al.* [8] proposed the limit surface force-motion model of the sliding system; Cutkosky *et al.* [9] simplified the model by an ellipsoidal approximation; Zhou *et al.* [4] validated the system's differential flatness properties.

In parallel, several works have also been proposed to deal with the control of discontinuous pushing dynamic caused by mutable contact modes (i.e. sticking, sliding). Inspired by recent developments in contact-rich locomotion, frictional contacts could be efficiently handled by complementary constraints [10]. Moura *et al.* [5] applied the technique and built an MPCC-based framework for robust planning and control. Wang *et al.* [11] used an alternative approach of State-Triggered Constraints (STC) and achieved better trajectory tracking performance.

Most of the existing methods assume that the contact between the pusher and the slider is rigid and consistent [12]; While switching the contact positions makes it flexible to manipulate the object, the planning of such a formulation becomes more challenging as it is involved both the discrete contact and the continuous trajectory; To handle contact switches, Doshi *et al.* [3] proposed an exhaustive tree search method, Xue *et al.* [12] used the human demonstration to guide the planning. However, these methods are limited either in the number of contact switches or in generalization ability, which does not function in densely cluttered environments,

especially when the pushing trajectory is infeasible at the beginning if obstacles are not moved.

B. Manipulation Planning in Cluttered Environments

Existing works apply hierarchical planning, exhaustive tree search, and sampling-based approaches for manipulation planning in cluttered environments.

First, hierarchical approaches are introduced to break the task down into several steps; Gao *et al.* [13] and Nam *et al.* [14] solved the object rearrangement task by solving combinatorial optimization at high level and motion planning at low level; These partitions designed for prehensile manipulation may not be suitable for complex kinodynamic constraints in pushing. Second, tree search can handle prehensile and non-prehensile cases [3], [15], [16], but it is subject to the combination explosion and relies on task-specific heuristics for pruning. Third, sampling-based techniques are less sensitive to the branching factor and enable efficiently exploring high-dimensional search space and handling holonomic constraints [17]; However, such methods commonly need expensive tree extension processes for non-holonomic dynamics [18], for instance, the pushing system (which is due to solving non-trivial two-point Boundary Value Problems (BVPs) when connecting arbitrary states [19]); To tackle the problem, Webb *et al.* [18] proposed Kinodynamic RRT*, which uses an optimal controller for state connection; For general nonlinear systems, Goretkin *et al.* [20] applied local approximation on dynamic constraints and cost function.

Different from the above approaches which assume continuous dynamics, the pushing system includes hybrid dynamics. Our work is inspired by utilizing reachable sets to guide the tree expansion [21], [22] and further extends the approach to pushing manipulation.

In summary, existing methods for manipulation planning in cluttered environments are commonly limited by several open issues: hybrid dynamics due to contact face switching and contact mode scheduling [23], pushing manipulation with fewer DoFs [24], obstacles with irregular shapes [5], [25], and heavy physics engines and large datasets [24]. Those issues will be systematically addressed in this paper.

III. METHOD

In this section, we formally define the planar object retrieval task and propose the contact-aware planning algorithm in Sec. III-A. Implementation of the contact-aware feature requires the computation of reachable sets for guided search (Sec. III-B.2), the object interaction module for motion prediction (Sec. III-C), and a robust feedback controller for trajectory tracking (Sec. III-D). The block diagram of the proposed framework is depicted in Fig. 2.

A. Pushing Task and Pushing Planner

1) *Problem Formulation:* This paper considers a planar workspace with the target object (also referred to as the planar slider) o^s and multiple fixed or movable obstacles denoted as $o_1^t, \dots, o_{|O^t|}^t \in O^t$ and $o_1^m, \dots, o_{|O^m|}^m \in O^m$, respectively. We assume the target object and obstacles are

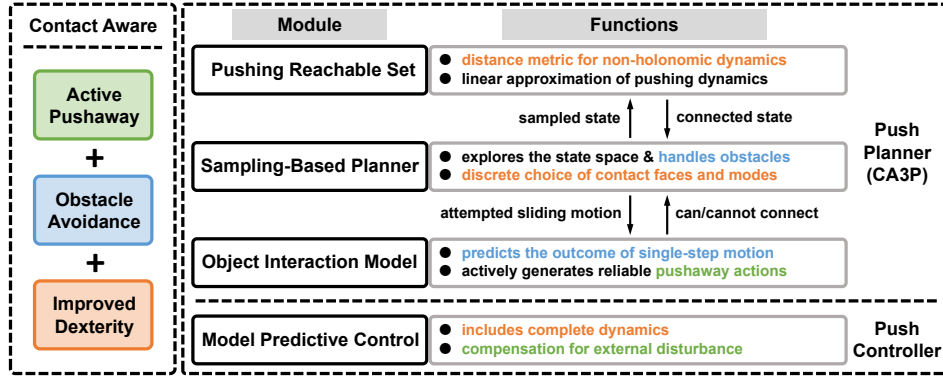


Fig. 2. Block diagram of the proposed framework (the planner and controller). Elements and implementations of the contact-aware feature are highlighted.

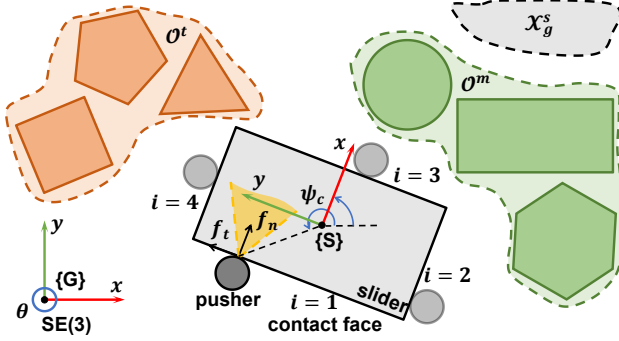


Fig. 3. Graphical representation of the planar object retrieval task, including the target object (planar slider) painted in grey, the goal region X_g^s , movable obstacles O^m and fixed obstacles O^t , $i \in \{1, 2, 3, 4\}$ denotes the discrete choice of contact face. Yellow shade represents the friction cone constraints.

convex polygons with known geometric parameters and their initial poses are also given. The target object is actuated by a single rod-like pusher p through frictional point contact, with friction coefficient μ_p . A graphical representation of the task is shown in Fig. 3. Note that the retrieval task in most of the existing works is to solve the control sequence which drives the target object from initial pose $x^s[0]$ to goal region $X_g^s \subset X^s$, without collision with all obstacles $O^t \cup O^m$.

This paper additionally considers actively utilizing contacts with the environment to create or amplify the pushing path. Hence, we consider solving the task in the joint state space $X^E = X^s \times X_1^m \times \dots \times X_{|O_m|}^m$, where \times denotes the Cartesian product. A state $x^E = (x^s, x_1^m, \dots, x_{|O_m|}^m)$ is called feasible if the fixed obstacles are not in contact with other objects (i.e., in case of turning over objects or getting stuck). The state transition is regulated by pushing dynamics (III-B.1) and the object interaction model (III-C).

Hence, the objective of this paper is to find the feasible state sequence $x^s[0 : T]$ and corresponding control sequence $u^p[0 : T - 1]$ which drives the target object to goal region, T is the path length. Note that the joint states $x^E[0 : T]$ which contain $x^s[0 : T]$ should all be feasible.

2) **Contact-Aware Pushing Planner:** The **Contact-Aware Planar Push Planner (CA3P)** is outlined in Algorithm 1. An illustration of the CA3P is given in Fig. 4 Left. Above all, the contact-aware feature could be divided into **three levels**. Specifically, the active avoidance and clearance of obstacles, and the contact face-switching technique to increase dexterity.

The proposed algorithm is derived from the RRT planner. The search tree of RRT is stored in \mathcal{H}^s , each node in \mathcal{H}^s records a feasible pose of the target object and the corresponding control input. To push aside movable obstacles to widen the pushing path and avoid other obstacles, we simultaneously track the changeable poses of O^m and the poses of O^t in \mathcal{H}^o , which is referred to as the **planning scene**. Note that \mathcal{H}^s and \mathcal{H}^o are identical in structure, which can be seen in Fig. 4 Left.

Since the pushing system is subject to non-holonomic constraints, the Euclidean distance works poorly; we adopt the concept of reachable sets [22] as a distance metric. In Algorithm 1, **NearestNeighbor** computes the nearest state x_{near} in all reachable sets of states in \mathcal{H}^s to a newly sampled state x_{new} (Line 5). We omit the superscript s of the target object for brevity. Then, **GetGenerateState** returns the **generating state** x_{gen} of the reachable set which contains x_{near} (Line 6). The notations and computation of reachable sets will be presented in Sec. III-B.2. Next, **Connect** calculates the control input u driving the system from x_{gen} to x_{near} (Line 7). Due to the linearization error of pushing dynamics, the rollout of u usually does not reach x_{near} exactly; We denote the actual terminal state as x_{term} . The state connection is realized by applying the discrete-time Linear-Quadratic Regulator (LQR) controller to the linear system:

$$x[k+1] = I_4 x[k] + (\tau_{\text{LQR}} B) u[k] \quad (1)$$

with step size τ_{LQR} , state cost C_Q and input cost C_R . The input matrix B will be further defined in Sec. III-B.2, the subscript i is also ignored for brevity.

The core procedure that enables the active clearance of obstacles is **Simulate** (Line 9), which predicts the outcome (i.e., new obstacle poses) of one-step target object motion. **GetEnviron** first queries the **planning scene** $\mathcal{O}_{\text{gen}}^m$ correlated with x_{gen} in \mathcal{H}^o (Line 8). Next, the configuration of the movable obstacles is updated through the object interaction model in Sec. III-C. The state connection is abandoned if collision with fixed obstacles is detected. If the state connection is successful, the search tree is updated with new **planning scene** $\text{Update}(\mathcal{O}_{\text{gen}}^m)$.

The abovementioned procedure is repeated until the maximum number of nodes is exceeded. Finally, the control

Algorithm 1: CA3P

Input: State space \mathcal{X}^s , obstacles $\mathcal{O}^t, \mathcal{O}^m$, initial pose $\mathbf{x}[0]$, goal region \mathcal{X}_g

Output: Control sequence $\mathbf{u}[0 : T - 1]$

Parameters: Reachable set step size τ , LQR step size τ_{LQR} , maximum number of nodes n_{max}

```

1 while not maximum number of nodes exceeded do
2   Initialize search tree  $\langle \mathcal{H}^s, \mathcal{H}^o \rangle$ ;
3    $\mathcal{H}^s.\text{nodes.add}((\mathbf{x}[0], \emptyset))$ ,  $\mathcal{H}^o.\text{nodes.add}(\mathcal{O}^t \cup \mathcal{O}^m)$ ;
4   Randomly sample  $\mathbf{x}_{\text{new}} \in \mathcal{X}^s$ ;
5    $\mathbf{x}_{\text{near}} \leftarrow \text{NearestNeighbor}(\mathbf{x}_{\text{new}}, \bigcup_{\mathbf{x} \in \mathcal{H}^s.\text{nodes}} \mathcal{R}_\tau(\mathbf{x}))$ ;
6    $\mathbf{x}_{\text{gen}} \leftarrow \text{GenerateState}(\mathbf{x}_{\text{near}})$ ;
7    $\mathbf{x}_{\text{term}}, \mathbf{u}[0 : \tau] \leftarrow \text{Connect}(\mathbf{x}_{\text{gen}}, \mathbf{x}_{\text{near}})$ ;
8    $\mathcal{O}_{\text{gen}}^t \cup \mathcal{O}_{\text{gen}}^m \leftarrow \text{GetEnviron}(\mathcal{H}^o.\text{nodes}, \mathbf{x}_{\text{gen}})$ ;
9   if  $\text{Simulate}(\mathbf{x}_{\text{gen}}, \mathbf{u}[0 : \tau], \mathcal{O}_{\text{gen}}^m, \mathcal{O}_{\text{gen}}^t)$  then
10     $\mathcal{H}^s.\text{nodes.add}((\mathbf{x}_{\text{term}}, \mathbf{u}[0 : \tau]))$ ;
11     $\mathcal{H}^s.\text{edges.add}((\mathbf{x}_{\text{gen}}, \mathbf{x}_{\text{term}}))$ ;
12     $\mathcal{H}^o.\text{nodes.add}(\mathcal{O}_{\text{gen}}^t \cup \text{Update}(\mathcal{O}_{\text{gen}}^m))$ ;
13     $\mathcal{H}^o.\text{edges.add}((\mathbf{x}_{\text{gen}}, \mathbf{x}_{\text{term}}))$ ;
14    if  $\text{Connect}(\mathbf{x}_{\text{term}}, \mathcal{X}_g)$  then
15      return  $\text{ExtractPath}(\mathcal{X}_g, \mathcal{H}^s)$ ;
16    end
17  end
18 end
19 return  $\emptyset$ ;

```

sequence $\mathbf{u}[0 : T - 1]$ is extracted from \mathcal{H}^s if the goal region \mathcal{X}_g is reachable from current states (Line 15).

B. Pushing Reachable Sets

In this subsection, we first introduce the dynamic model and constraints of planar pushing and then present the computation of reachable sets, including an approximation to the dynamics.

1) *Pushing Dynamics:* As seen in (3), state variables of the dynamic model can be chosen as the configuration of the planar slider and pusher

$$\mathbf{x}^s \triangleq [x^s, y^s, \theta^s, \psi_c]^T, \quad (2)$$

where x^s, y^s, θ^s denote the position and the orientation of the slider (i.e., target object) with respect to the global frame, and $\psi_c \in [-\pi, \pi]$ is the azimuth angle of the pusher's contact point on the slider's periphery.

Input variables include the pusher's contact force and velocity

$$\mathbf{u}^p \triangleq [f_n, f_t, \dot{\psi}_c]^T, \quad (3)$$

where f_n, f_t represent the normal and tangential forces at the slider's local coordinates. The concept of limit surface proposed by Goyal *et al.* [8] maps the frictional wrench \mathcal{F}^s to the slider's twist \mathcal{V}^s : $\mathcal{V}^s = \mathbf{A}\mathcal{F}^s$, where \mathbf{A} is a positive definite matrix defined by the maximum frictional wrench that can be exerted on the slider.

Under quasi-static assumptions, the system dynamics model can now be given as

$$\dot{\mathbf{x}}^s = \mathbf{f}_i(\mathbf{x}^s, \mathbf{u}^p) \triangleq \begin{bmatrix} \mathbf{R}\mathbf{A}\mathbf{J}_{c,i}^\top & 0 \\ 0 & 1 \end{bmatrix} \mathbf{u}^p, \quad (4)$$

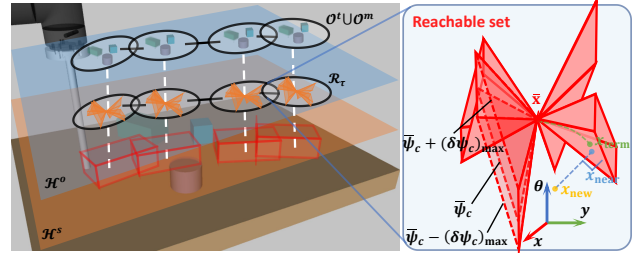


Fig. 4. Illustration of the CA3P search trees and the reachable set. **Left:** reachable sets \mathcal{R}_τ and planning scenes $\mathcal{O}^t \cup \mathcal{O}^m$ are stored in trees of the same structure, denoted as \mathcal{H}^s and \mathcal{H}^o . **Right:** the reachable set is composed of several convex cones; each cone corresponds to pushing a certain contact face. Each *slice* of the cone is with a fixed contact point location, e.g., $\bar{\psi}_c - (\delta\psi_c)_{\max}, \bar{\psi}_c, \bar{\psi}_c + (\delta\psi_c)_{\max}$. Generating state $\bar{\mathbf{x}}$ of the reachable set, the sampled state \mathbf{x}_{new} , nearest neighbor \mathbf{x}_{near} , and terminal state \mathbf{x}_{term} reached by state connection are shown.

where $i = 1, \dots, N$, N is the number of contact faces, \mathbf{R} is the rotation matrix from the slider's local coordinates to global coordinates, and $\mathbf{J}_{c,i}$ is the contact jacobian. The subscript i is introduced to denote the discontinuous dynamics due to switching contact face, as illustrated in Fig. 3.

In practice, the state variables are constrained in the workspace $\mathbf{x}^s \in \mathcal{X}^s$, and the input variables are subject to box constraints and Coulomb friction constraints. We define $\mathcal{U}_f : 0 \leq f_n \leq \bar{f}, \mathcal{U}_{\psi+} : \dot{\psi}_c > 0, \mathcal{U}_{\psi-} : \dot{\psi}_c < 0$ such that

$$\mathcal{U}_{st} : \begin{cases} \mathcal{U}_f \\ |f_t| \leq \mu_p f_n \\ \dot{\psi}_c = 0 \end{cases}, \mathcal{U}_{sl} : \begin{cases} \mathcal{U}_f, \mathcal{U}_{\psi-} \\ f_t = \mu_p f_n \\ -\bar{\psi}_c \leq \dot{\psi}_c \end{cases}, \mathcal{U}_{sr} : \begin{cases} \mathcal{U}_f, \mathcal{U}_{\psi+} \\ f_t = -\mu_p f_n \\ \dot{\psi}_c \leq \bar{\psi}_c \end{cases} \quad (5)$$

where $\bar{f}, \bar{\psi}_c$ are upper bounds of the pusher's contact force and velocity, $\mathcal{U}_{st}, \mathcal{U}_{sl}$ and \mathcal{U}_{sr} represent the input constraints for sticking, sliding left and sliding right contact modes respectively, and μ_p is the friction coefficient between pusher and slider.

2) *Computation of Reachable Sets:* The reachable sets highlight the states more likely to be connected from the already explored state space. This technique can provide directional guidance to kinodynamic push planning. The reachable sets of arbitrary state $\bar{\mathbf{x}} \in \mathcal{X}$ is defined as the set of states reachable from $\bar{\mathbf{x}}$ within finite time horizon τ , under the dynamic constraints and constraints on state and input variables:

$$\mathcal{R}_\tau(\bar{\mathbf{x}}) \triangleq \{ \mathbf{x} \in \mathcal{X} | \exists (x, u) : [0, t] \mapsto (\mathcal{X}, \mathcal{U}), t \in [0, \tau], \mathbf{x}(0) = \bar{\mathbf{x}}, \mathbf{x}(\tau) = \mathbf{x}, \dot{\mathbf{x}}(\xi) = \mathbf{f}_i(\mathbf{x}(\xi), \mathbf{u}(\xi)) \}. \quad (6)$$

We call $\bar{\mathbf{x}}$ the **generating state** of the **reachable set** $\mathcal{R}_\tau(\bar{\mathbf{x}})$. Using the time integration of (4), the terminal state is computed as

$$\mathbf{x}(t) = \bar{\mathbf{x}} + \int_0^t \mathbf{f}_i(\mathbf{x}(\xi), \mathbf{u}(\xi)) d\xi \quad (7)$$

Note that due to nonlinear pushing dynamics (4), the analytic representation of (7) is hard to obtain, and so is (6).

Assuming τ is small, it is reasonable to make a linear approximation of (4) at state $\bar{\mathbf{x}}$ and input $\bar{\mathbf{u}}$ as

$$\mathbf{f}_i(\mathbf{x}, \mathbf{u}) \approx \mathbf{f}_i(\bar{\mathbf{x}}, \bar{\mathbf{u}}) + \mathbf{A}_i(\mathbf{x} - \bar{\mathbf{x}}) + \mathbf{B}_i(\mathbf{u} - \bar{\mathbf{u}}), \quad (8)$$

where $A_i = \frac{\partial}{\partial x} f_i(x, u) \Big|_{(\bar{x}, \bar{u})}$, $B_i = \frac{\partial}{\partial u} f_i(x, u) \Big|_{(\bar{x}, \bar{u})}$, note that $A_i = 0$ for $\bar{u} = 0$.

In addition, we rewrite the input constraints in (5) as linear inequalities:

$$\mathcal{U}_j = \{u | D_j u \leq h_j\}, j \in \{st, sl, sr\}, \quad (9)$$

and assume u is invariant over the considered time horizon τ , $\bar{u} = 0$, thus an approximation to the **terminal states** (7), corresponding to the i^{th} contact face and the j^{th} contact mode, under all possible inputs are formulated as a set:

$$\mathcal{T}_\tau(\bar{x})_{ij} = \{x | x = \bar{x} + \tau B_i u, u \in \mathcal{U}_j\}. \quad (10)$$

Since we apply the linearized dynamics of (4), x , y and θ are independent of $\dot{\psi}_c$, the change of contact location ψ_c does not affect the (x, y, θ) dimensions of the reachable set, leading to an over-conservative approximation. To consider the influence of the pusher's movement on the slider's periphery, we consider all possible contact point locations during time horizon τ , that is, $\psi_c \in \mathcal{P} = [\bar{\psi}_c - (\delta\psi_c)_{max}, \bar{\psi}_c + (\delta\psi_c)_{max}]$, where $(\delta\psi_c)_{max} = \tau\dot{\psi}_c$. Hence an expansion of (10) is of the following form:

$$\mathcal{AT}_\tau(\bar{x})_{ij} = \bigcup_{\psi_c \in \mathcal{P}} \mathcal{T}_\tau([\bar{x}, \bar{y}, \bar{\theta}, \psi_c])_{ij}. \quad (11)$$

Proposition 1. $\forall \bar{x} \in \mathcal{X}, \bar{u} = 0, \tau \geq 0$, the expanded set of terminal states \mathcal{AT} in (11) is convex.

Proof. We prove the convexity of \mathcal{AT} by showing the union of $B_i u$ with $\psi_c \in \mathcal{P}$ is convex. According to (4) and (8), such $B_i u$ can be expressed as the Cartesian product $\mathcal{S}_1 \times \mathcal{S}_2$, where $(x, y, \theta) \in \mathcal{S}_1$ and $\psi_c \in \mathcal{S}_2$. From (10), we know \mathcal{S}_2 is an affine transformation of \mathcal{U} and hence is convex. In addition, we denote $[RAJ_c^\top; 0]$ as $[C_1; C_2(\psi_c)]$, where $C_1 \in \mathbb{R}^{2 \times 4}$ is constant matrix and $C_2 \in \mathbb{R}^{1 \times 4}$ is a continuous function of ψ_c . Assume $l \in [0, 1]$, $x_1, x_2 \in \mathcal{S}_1$, $x(l) = lx_1 + (1-l)x_2$, then $\exists \psi_{c,1}, \psi_{c,2} \in \mathcal{P}$, $u_1, u_2 \in \mathcal{U}$, such that $x_1 = [C_1; C_2(\psi_{c,1})]u_1$, $x_2 = [C_1; C_2(\psi_{c,2})]u_2$, and their convex combination $x(l) = [C_1 u(l); lC_2(\psi_{c,1})u_1 + (1-l)C_2(\psi_{c,2})u_2]$. Since C_2 is continuous, $C_2 u$ is monotonic, $\exists \psi_c^* \in \mathcal{P}$, such that $lC_2(\psi_{c,1})u_1 + (1-l)C_2(\psi_{c,2})u_2 = C_2(\psi_c^*)u(l)$, where $u(l) = lu_1 + (1-l)u_2 \in \mathcal{U}$. So far, the convexity of \mathcal{S}_1 and \mathcal{AT} are proved. \square

Based on (11), we can obtain the analytic approximation of (6) as:

$$\mathcal{R}_\tau(\bar{x}) \approx \bigcup_{\substack{i=1, \dots, N \\ j \in \{st, sl, sr\}}} \mathcal{AT}_\tau(\bar{x})_{ij}, \quad (12)$$

an example of such a set is shown in Fig. 4 **Right**. The reachable set contains new slider poses to be reached from a certain pose with greater probability and naturally enables a discrete choice of the contact face and mode. Since it is still the union of multiple convex sets, computationally efficient methods can be derived for nearest neighbor search [22].

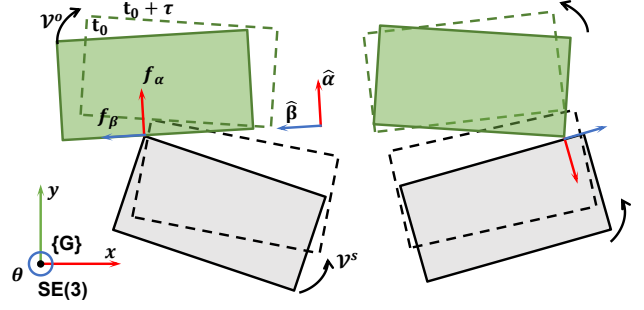


Fig. 5. Two different configurations of object interaction. $\mathcal{V}^s, \mathcal{V}^o$ are instantaneous twists, $\hat{\alpha}, \hat{\beta}$ are the contact normal and tangential, $f_\alpha, f_\beta = f_{\beta+} - f_{\beta-}$ are contact forces. **Left:** $\hat{\alpha}$ points inwards the obstacle (painted in green). **Right:** $\hat{\alpha}$ points inwards the slider (painted in grey).

C. Object Interaction Model

The object interaction model is designed to forecast the motion of movable objects in contact with the planar slider. Fixed objects in Sec. III-A.1 refer to objects that fall over easily under unintentional contacts. It is dangerous to enable interaction with these objects in planning, even with the physics engine, because control error may lead to large divergence. Besides, relying on a physics engine for precise motion prediction is time-consuming and unnecessary.

We denote the contact normal and tangential as $\hat{\alpha}$ and $\hat{\beta}$. Without loss of generality, we assume $\hat{\alpha}, \hat{\beta}$ form a right-handed coordinate system, and $\hat{\alpha}$ points inwards the obstacle, as seen in Fig. 5 **Left**. The contact force is defined as $f = [f_\alpha, f_{\beta+}, f_{\beta-}]^\top \succeq 0$. Given the twist of slider and obstacle in global coordinates $\mathcal{V}^s, \mathcal{V}^o$, and the contact jacobians J_c^s, J_c^o , the non-penetration constraints can be expressed as:

$$\begin{aligned} 0 &\leq \hat{\alpha}^\top (J_c^o \mathcal{V}^o - J_c^s \mathcal{V}^s) \perp f_\alpha \geq 0 \\ 0 &\preceq \begin{bmatrix} \hat{\beta}^\top \\ -\hat{\beta}^\top \end{bmatrix} (J_c^o \mathcal{V}^o - J_c^s \mathcal{V}^s) + \lambda \begin{bmatrix} 1 \\ 1 \end{bmatrix} \perp \begin{bmatrix} f_{\beta+} \\ f_{\beta-} \end{bmatrix} \succeq 0. \quad (13) \\ 0 &\leq \mu f_\alpha - f_{\beta+} - f_{\beta-} \perp \lambda \geq 0 \end{aligned}$$

Hence, the feasible contact force that satisfies the constraints in (13) is equivalent to the solution of the Linear Complementarity Problem (LCP):

$$\begin{aligned} z &= \begin{bmatrix} M^\top K^o M & 0 \\ \mu & -1^\top \\ 0 & 0 \end{bmatrix} \begin{bmatrix} f \\ \lambda \end{bmatrix} + \begin{bmatrix} -M^\top J_c^s \mathcal{V}^s \\ 0 \end{bmatrix}, \quad (14) \\ 0 &\preceq z \perp \begin{bmatrix} f \\ \lambda \end{bmatrix} \succeq 0 \end{aligned}$$

where z is the auxiliary variable, $M = [\hat{\alpha}, \hat{\beta}, -\hat{\beta}]$, and $K^o = J_c^o A J_c^{o\top}$ maps the contact force to contact point velocity. The LCP (14) can be efficiently solved with Newton-based methods [26]. Then, new poses of the movable obstacle $o_k^m \in \mathcal{O}^m$ can be obtained through forward integration:

$$x_k[t_0 + \tau] = x_k[t_0] + \tau R(\theta_k[t_0]) A J_c^{o\top} M f, \quad (15)$$

where $R(\theta_k[t_0]) \in \mathbb{R}^{3 \times 3}$ is the rotation matrix. Similar conclusions as (13)~(15) can be drawn for a different scenario in Fig. 5 **Right**, where $\hat{\alpha}$ points inwards the slider.

Based on the abovementioned techniques, the lightweight interaction model (13)~(15) balances safety and efficiency in push planning.

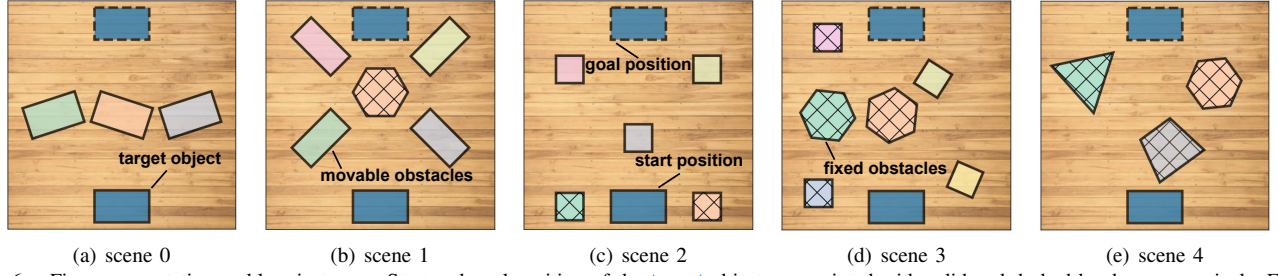


Fig. 6. Five representative problem instances. Start and goal position of the **target** objects are painted with solid and dashed borders, respectively. Fixed obstacles are marked with net mesh. The tasks in **scene 0** and **scene 1** require the obstacles to be cleared away. The search process for **scene 2** and **scene 3** can be accelerated by pushing aside the obstacles, although not essential. **Scene 4** only needs obstacle avoidance.

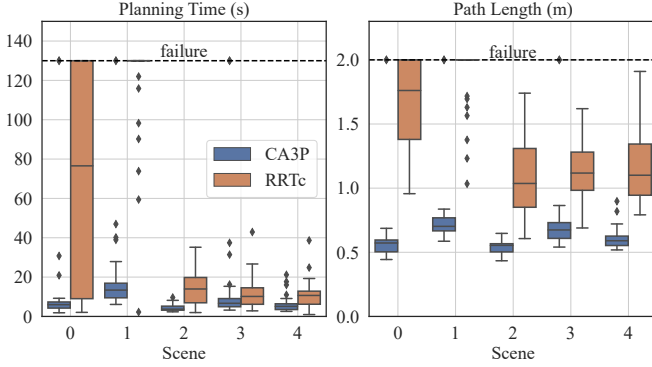


Fig. 7. Results of CA3P and RRTc on five instances across 30 trials. The planning time and path length are set as 130s and 2.0m for failure trials. The median, lower and upper quartiles, error bars, and outlier values are reported. Less planning time means the method is more efficient. A shorter path length means the result is more optimal.

D. Model Predictive Pushing Controller

To execute trajectories planned by CA3P, we adopted the Math Programming with Complementarity Constraints (MPCC) formulation in [5] with compensation of external disturbance, which refers to the additional contact force during interaction with movable obstacles. The disturbance is modeled as a time-varying term in the nominal dynamics

$$\dot{\mathbf{x}}(t) = \mathbf{f}(\mathbf{x}(t), \mathbf{u}(t)) + \hat{\mathbf{d}}(t). \quad (16)$$

The dynamic constraints in MPCC are compensated by the estimated disturbance

$$\mathbf{x}[k+1] = \mathbf{x}[k] + \tau_{\text{MPC}} \left[\mathbf{f}(\mathbf{x}[k], \mathbf{u}[k]) + \hat{\mathbf{d}}[k] \right], \quad (17)$$

where τ_{MPC} is the control time step. The estimated disturbance is updated as

$$\hat{\mathbf{d}}[k] = \kappa_d (\mathbf{x}_{\text{obs}}[k] - \mathbf{x}_{\text{mpc}}[k]), \quad (18)$$

where $\mathbf{x}_{\text{obs}}[k]$, $\mathbf{x}_{\text{mpc}}[k]$ are observed and predicted states, respectively, $\kappa_d > 0$ denotes the update rate. The compensation for contact force reinforces closed-loop feedback and avoids modeling the multi-slider control problem with complex nonlinear MPC.

IV. RESULTS

In this section, we show that CA3P generates a shorter path in less time compared with baselines, utilizing the contact-aware feature. Moreover, we demonstrate through robot experiments that the proposed algorithm is capable of executing the planned path with an acceptable error, even if the slider is obstructed by obstacles.

TABLE I
SUCCESS RATE AND NUMBER OF NODES

Scene	0	1	2	3	4
Success	CA3P 28/30 RRTc 19/30	28/30 7/30	30/30 30/30	28/30 30/30	30/30 30/30
• Node In Tree	CA3P 263±219 RRTc 107±117	544±347 302±160	169±67 25±14	286±242 22±12	210±135 31±21

• reported as mean±standard deviation.

A. Simulation Studies

The simulations were conducted on a 64-bit Intel Core i7-12700 4.9GHz Ubuntu workstation with 32GB RAM. We used Shapely [27] for collision detection and visualization. We compared CA3P with the following baselines:

1) *RRTc*: An RRT-based planner utilizing the differential flatness properties proposed in [4]. The slider is manipulated through sticking contacts and forced to follow trajectories with constant curvature, i.e., Dubins path. Whenever a new sample and its nearest neighbor are generated, the corresponding contact point (including the contact face) and force direction are obtained through differential flat mapping. We hypothesize that this method imposes tight constraints on motion planning and could hardly find a nearly optimal path.

2) *MPCC*: The optimization-based scheme proposed in [5], which uses nonlinear programming with obstacle avoidance constraints. Since this method is difficult to solve with the number of obstacles we considered, we approximated the obstacles by their maximum inscribed circles to make more space. We hypothesize that this method is less flexible when handling obstacles.

For CA3P, we set the goal sampling bias as 0.1, and set $\bar{f} = 0.15 \text{ N}$, $\bar{\psi}_c = 1.0 \text{ rad/s}$, $\mu_p = 0.2$, $\tau = 0.05 \text{ s}$, $\tau_{\text{LQR}} = 0.01 \text{ s}$. For all methods, we define the stopping criterion as maximum planning time $1 \times 10^3 \text{ s}$ or maximum number of nodes 1×10^3 . A method will return failure if the goal region is unreachable from explored states when the criterion is met. To evaluate the effectiveness of the proposed method, we generated 5 representative problem instances, as shown in Fig. 6. The planning time and total path length for each instance across 30 trials are shown in Fig. 7, and the success rate and the number of nodes are presented in Table. I.

The proposed CA3P greatly reduced planning time and generated shorter trajectories. Moreover, CA3P reports narrower interquartile ranges for all problem instances, indicating that the method achieves more stable performance with random scenes and trials. For more complicated scene 0 and scene 1, CA3P increased the success rate by 30% and 70%. We

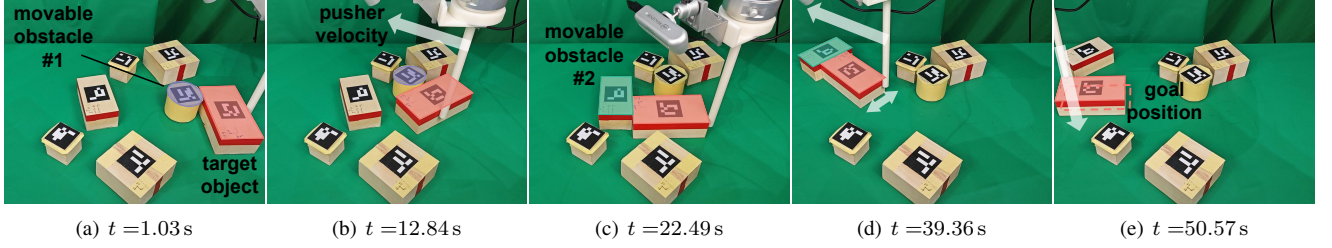


Fig. 8. Snapshots of the planar object retrieval task executed on a UR5 robot arm. The slider was manipulated to consecutively push aside a cylindrical (a-b) and a cubic obstacle (c-d) and was finally pushed to the goal position after switching contact faces. The time consumed on switching faces is ignored.

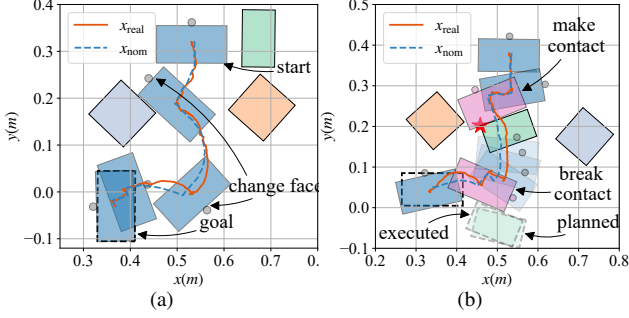


Fig. 9. Planned (nominal) and executed trajectory of the planar slider. Several keyframes before switching faces are depicted with the round pusher. (a) Obstacle avoidance. (b) Removal of the green object through pushing.

observed that RRTc completed all the trials if the search space was enlarged by 40% on each side, at the expense of adding 20% to trajectory length. Nevertheless, such a compromise is impractical due to the constrained environment and limited workspace of the manipulator. Results of scene 2 and scene 3 showed that actively removing obstacles is an effective way to obtain consistent path length; since avoiding obstacles is pretty demanding in the sampling sequence and quality. Results of scene 4 proved that the reachable set offers preferable directions in the search process.

Whatever we did to adjust the parameters and manually decide the contact face, the MPCC baseline failed to solve all the problem instances, either due to collision or the large distance towards the goal. The result is mainly because the controllability of the planar slider is significantly restricted if it is not allowed to switch contact faces.

B. Real-World Experiments

We implemented the robot experiments on a 64-bit Intel Core i7-9700 4.7GHz Ubuntu workstation with 16GB RAM. We mounted a $\Phi 15 \times 250$ mm resin pusher on a UR5 robot. The perception system was composed of an Intel Realsense D435i camera and several ArUco markers.

The effectiveness of the proposed method was demonstrated through an obstacle avoidance task; and a task where the removal of obstacles is required. In both tasks, the planar slider was $8.0 \times 15.0 \times 5.0$ cm³ in size, with estimated $\mu_p = 0.1$ and measured frictional force 1.2 N. The movable obstacle was a $7.0 \times 12.2 \times 5.0$ cm³ cube. Finally, we tested the algorithm in a planar object retrieval task to validate the possibility of generalizing the method to obstacles of other geometric shapes, i.e., cylinders, and to validate the robustness when consecutively pushing away obstacles is needed. In all the experiments, the MPC prediction horizon was 30 steps,

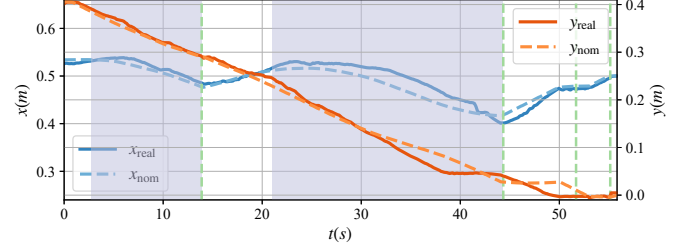


Fig. 10. Tracking error of the object retrieval task. Green dashed lines mark the moments of switching faces; purple shadows report the intervals of contact. Blue and orange curves represent the x and y dimensions, respectively.

and we set $\bar{f} = 0.5$ N, $\bar{\psi}_c = 3.0$ rad/s, $\tau_{MPC} = 0.04$ s, and set $\bar{\psi}_c = 0.52, 0.9$ rad for the short and long edge of the slider, respectively. The planned path, pusher, and slider trajectories in the obstacle avoidance task are presented in Fig. 9(a). It is hard for the slider to move through the obstacles in its initial pose because the interspace is narrower than the side length. Hence, the slider steered to have a short edge ahead. Note that the task requires sharp turning at times, which relies on the face-switching technique to improve controllability. There were no redundant movements of the slider except for near the target, which can be further improved by replacing the goal pose with the goal region. As shown in Fig. 9(b), the slider is obstructed by one movable obstacle and two square objects fixed on either side. To make space and simultaneously approach the goal, the slider contacted, pushed, and detached from the obstacle in succession. Despite the inaccurate modeling and randomness of frictional contacts, there is not much difference in the final positions of the movable obstacle between execution and planning. Moreover, the disturbance rejection property of MPC allowed the system to recover from moderate tracking errors. As seen in Fig. 9(b), the pusher moved towards the edge of the contact face to increase the moment of the exerted force. Then, the slider successfully reached the target position with a small error; since the tracking error remained bounded in continuous contact and rapidly converged once the disturbance vanished.

Finally, Fig. 8 depicts five keyframes of a complete planar object retrieval task. The initial and goal positions of the planar slider are $\mathbf{x}^s[0] = [0.53 \text{ m}, 0.41 \text{ m}, -1.57 \text{ rad}]^T$ and $\mathbf{x}^s[T] = [0.50 \text{ m}, 0.00 \text{ m}, -3.14 \text{ rad}]^T$, respectively. The task scenerio contains fixed obstacles of $10.0 \times 10.2 \times 5.0$ cm³ and $5.0 \times 5.0 \times 5.0$ cm³, the additional cylindrical movable obstacle is of $\Phi 7 \times 6$ cm³. Obstacles are simplified as their minimum bounding rectangles in CA3P, with an estimated frictional coefficient $\mu = 0.3$ between all pairs. Since it is challenging to control contact forces directly, we converted the control

input u^p to speed command. The pusher is initialized at the center of each contact face the robot has switched to. Other parameters remain unchanged compared to the two previous experiments. As shown in Fig. 8(a) and Fig. 8(b), the slider pushed the cylindrical object aside to enlarge the space ahead; instead of passively performing a time-consuming avoidance behavior. Later the slider passed through the narrow corridor and came into contact with another obstacle, as Fig. 8(c) depicts. We observed the fast-moving behavior of the pusher on the slider's periphery as an anti-disturbance mechanism (Fig. 8(d)). The slider eventually broke out of the clutter in 50.6 s (Fig. 8(e)). The tracking error in the x and y directions are reported in Fig. 10.

V. CONCLUSIONS

This work proposes a new manipulation method for non-prehensile planar pushing in a constrained workspace. We combine sampling-based approaches with a simplified object interaction model for motion planning and apply the MPC scheme for robust control. With the use of those techniques together, the proposed method is with the novel contact-aware feature, which allows the robot to actively avoid obstacles, switch contacts, or remove obstacles simultaneously. Multiple actions are integrated into the planning algorithm of CA3P, and its effectiveness has been comprehensively validated in the task of object retrieval, subject to several challenges (e.g., densely cluttered environments, uncertain physical parameters, and complex kinodynamic constraints). Future works will be devoted to improving the quality of motion planning with trajectory optimization; and to taking account of higher-order dynamics for preferable dynamic non-prehensile manipulation.

REFERENCES

- [1] M. T. Mason, "Progress in nonprehensile manipulation," *The International Journal of Robotics Research*, vol. 18, pp. 1129 – 1141, 1999.
- [2] F. Ruggiero, V. Lippiello, and B. Siciliano, "Nonprehensile dynamic manipulation: A survey," *IEEE Robotics and Automation Letters*, vol. 3, no. 3, pp. 1711–1718, 2018.
- [3] N. Doshi, F. R. Hogan, and A. Rodriguez, "Hybrid differential dynamic programming for planar manipulation primitives," *2020 IEEE International Conference on Robotics and Automation (ICRA)*, pp. 6759–6765, 2019.
- [4] J. Zhou, Y. Hou, and M. T. Mason, "Pushing revisited: Differential flatness, trajectory planning, and stabilization," *International Journal of Robotics Research: Special Issue on ISRR '17*, vol. 38, no. 12, pp. 1477 – 1489, September 2019.
- [5] J. Moura, T. Stouraitis, and S. Vijayakumar, "Non-prehensile planar manipulation via trajectory optimization with complementarity constraints," *2022 International Conference on Robotics and Automation (ICRA)*, pp. 970–976, 2021.
- [6] C.-Y. Chai, W. Peng, and S.-L. Tsao, "Object rearrangement through planar pushing: A theoretical analysis and validation," *IEEE Transactions on Robotics*, vol. 38, pp. 2703–2719, 2022.
- [7] M. T. Mason, "Manipulator grasping and pushing operations," January 1982.
- [8] S. Goyal, A. Ruina, and J. Papadopoulos, "Planar sliding with dry friction part 1. limit surface and moment function," *Wear*, vol. 143, no. 2, pp. 307–330, 1991.
- [9] S. H. Lee and M. R. Cutkosky, "Fixture Planning With Friction," *Journal of Engineering for Industry*, vol. 113, no. 3, pp. 320–327, 08 1991.
- [10] J. Zhou, J. Bagnell, and M. Mason, "A fast stochastic contact model for planar pushing and grasping: Theory and experimental validation," in *Proceedings of Robotics: Science and Systems*, Cambridge, Massachusetts, July 2017.
- [11] M. Wang, A. Ö. Önel, P. Long, and T. Padir, "Contact-implicit planning and control for non-prehensile manipulation using state-triggered constraints," *ArXiv*, vol. abs/2210.09540, 2022.
- [12] T. Xue, H. Girgin, T. S. Lembono, and S. Calinon, "Demonstration-guided optimal control for long-term non-prehensile planar manipulation," *ArXiv*, vol. abs/2212.12814, 2022.
- [13] K. Gao, D. T. M. Lau, B. Huang, K. E. Bekris, and J. Yu, "Fast high-quality tabletop rearrangement in bounded workspace," *2022 International Conference on Robotics and Automation (ICRA)*, pp. 1961–1967, 2021.
- [14] C. Nam, S. H. Cheong, J. Lee, D. H. Kim, and C. Kim, "Fast and resilient manipulation planning for object retrieval in cluttered and confined environments," *IEEE Transactions on Robotics*, vol. 37, pp. 1539–1552, 2021.
- [15] H. Song, J. A. Haustein, W. Yuan, K. Hang, M. Y. Wang, D. Kragic, and J. A. Stork, "Multi-object rearrangement with monte carlo tree search: A case study on planar nonprehensile sorting," *2020 IEEE/RSJ International Conference on Intelligent Robots and Systems (IROS)*, pp. 9433–9440, 2019.
- [16] C. Chen, P. Culbertson, M. Lepert, M. Schwager, and J. Bohg, "Trajectory optimization meets tree search for planning multi-contact dexterous manipulation," *2021 IEEE/RSJ International Conference on Intelligent Robots and Systems (IROS)*, pp. 8262–8268, 2021.
- [17] X. Cheng, E. Huang, Y. Hou, and M. T. Mason, "Contact mode guided sampling-based planning for quasistatic dexterous manipulation in 2d," *2021 IEEE International Conference on Robotics and Automation (ICRA)*, pp. 6520–6526, 2020.
- [18] D. J. Webb and J. P. van den Berg, "Kinodynamic rrt*: Asymptotically optimal motion planning for robots with linear dynamics," *2013 IEEE International Conference on Robotics and Automation (ICRA)*, pp. 5054–5061, 2013.
- [19] C. Xie, J. P. van den Berg, S. Patil, and P. Abbeel, "Toward asymptotically optimal motion planning for kinodynamic systems using a two-point boundary value problem solver," *2015 IEEE International Conference on Robotics and Automation (ICRA)*, pp. 4187–4194, 2015.
- [20] G. Goretkin, A. Perez, R. W. Platt, and G. D. Konidaris, "Optimal sampling-based planning for linear-quadratic kinodynamic systems," *2013 IEEE International Conference on Robotics and Automation (ICRA)*, pp. 2429–2436, 2013.
- [21] A. C. Shkolnik, M. R. Walter, and R. Tedrake, "Reachability-guided sampling for planning under differential constraints," *2009 IEEE International Conference on Robotics and Automation (ICRA)*, pp. 2859–2865, 2009.
- [22] A. Wu, S. Sadraddini, and R. Tedrake, "R3t: Rapidly-exploring random reachable set tree for optimal kinodynamic planning of nonlinear hybrid systems," *2020 IEEE International Conference on Robotics and Automation (ICRA)*, pp. 4245–4251, 2020.
- [23] F. R. Hogan and A. Rodriguez, "Feedback control of the pusher-slider system: A story of hybrid and underactuated contact dynamics," in *Algorithmic Foundations of Robotics XII: Proceedings of the Twelfth Workshop on the Algorithmic Foundations of Robotics*. Springer, 2020, pp. 800–815.
- [24] Z. Wei, W. Chen, H. Wang, and J. Wang, "Manipulator motion planning using flexible obstacle avoidance based on model learning," *International Journal of Advanced Robotic Systems*, vol. 14, 2017.
- [25] C.-Y. Chai, W.-H. Peng, and S.-L. Tsao, "Adaptive unknown object rearrangement using low-cost tabletop robot," *2020 IEEE International Conference on Robotics and Automation (ICRA)*, pp. 2372–2378, 2020.
- [26] A. Fischer, "A newton-type method for positive-semidefinite linear complementarity problems," *Journal of Optimization Theory and Applications*, vol. 86, pp. 585–608, 1995.
- [27] S. Gillies, C. van der Wel, J. Van den Bossche, M. W. Taves, J. Arnott, B. C. Ward, and others, "Shapely," 1 2023. [Online]. Available: <https://github.com/shapely/shapely>